Full Numerical Simulations of Dynamical Response in Superconducting Single-Photon Detectors

Yukihiro Ota, Keita Kobayashi, Masahiko Machida, Tomio Koyama, and Franco Nori

(Invited Paper)

***Abstract*—We numerically study transport phenomena in a superconducting detector. Our approach is to simulate the three-dimensional time-dependent Ginzburg-Landau equation coupled with heat-diffusion and Maxwell equations. The simulation shows dynamical transition to a resistive state when an incident particle has energy higher than superconducting transition temperature. We show temporal behaviors of a superconducting gap function, depending on the incident energy scale. Furthermore, we discuss the applicability of our method to a superconducting single-photon detector. Focusing on the effects of coupling with heat sink and magnitude of quasi-particle fluctuations, we show a significant decrease of detector's threshold energy.**

***Index Terms*—Superconducting photodetectors, superconducting thin films.**

I. Introduction

SUPERCONDUCTIVITY allows interesting and useful devices, such as transition edge sensors [1], terahertz emitters [2], [3], magnets [4], Josephson qubits [5], [6], etc. A superconducting detector is one of these devices, and its effectiveness leads to sensitive detection of single photons [7]–[13], neutrons [14]–[16], molecules [17]–[19], etc. The physics in superconducting detectors is related to non-equilibrium transport phenomena and heating effects in nano-scale superconductors. Thus, a large-scale simulation is highly desirable for a systematic study of superconducting detectors.

Time-dependent Ginzburg-Landau (TDGL) formalism is one of the powerful methods to examine superconducting transport phenomena in the vicinity of $T_{\rm c}$, as seen in, e.g., [20]–[24]. Several studies about superconducting detectors with the TDGL approach were reported. Two of the present authors (MM and TK), Kato, and Ishida [14]–[16] have developed a method for studying a superconducting neutron detector in the vicinity of $T_{\rm c}$. Zotova and Vodolazov [25] simulated dynamical behaviors of a superconducting nanowire single-photon detector (SNSPD) using two-dimensional TDGL formulation. In contrast to the above study, their simulation was done at a low temperature ($\sim 0.5T_{\rm c}$), because SNSPDs typically operate at a temperature much less than $T_{\rm c}$ (see, e.g., [13]). However, a three-dimensional dynamical analysis of superconducting detectors at a very low temperature has been rarely performed.

In this paper, we numerically simulate a superconducting detector using the TDGL equation coupled with the heat-diffusion and the Maxwell equations [14]–[16], [22]. In order to develop a useful tool for evaluating the detector characteristics of a SNSPD, we perform three-dimensional full numerical simulations at a very low temperature ($0.3T_{\rm c}$). When an incident particle brings a large enough temperature increase, a superconductor dynamically transits to its resistive state. Furthermore, we discuss how the present simulation is related to a SNSPD.

II. System

We consider a SNSPD made of a NbN thin film which works at a temperature $T_{\rm w} = 3$ K. In this paper we focus on part of a superconducting nanowire, in order to study its basic working principle, although the real device [13] has a meandering structure. Also, its surrounding electric circuits are dropped. The spatial variables are normalized by the coherent length of NbN at $T = 0$. We denote it as $\xi(= 5$ nm). The film length (along x-axis) is 100ξ, and the film width (along y-axis) is 20ξ. The bias current flows into the direction of x-axis. The film thickness ($\|z$-axis) is set as 0.8ξ.

III. TDGL Approach

We simulate dynamical responses of a superconducting detector using the three-dimensional TDGL equation coupled with the heat-diffusion and Maxwell equations. Here, we briefly summarize our theoretical approach.

The dimensionless TDGL equation with respect to the superconducting gap function $\Delta(t, \vec{r})$ is

$$-D^{-1}\frac{\partial \Delta}{\partial t} = (-\mathrm{i}\vec{\nabla} - \vec{A})^2\Delta - (1-T)\Delta + |\Delta|^2\Delta + \zeta \quad (1)$$

Manuscript received October 5, 2012; accepted February 19, 2013. Date of publication February 25, 2013; date of current version March 22, 2013. The work of Y. Ota was supported in part by the Special Postdoctoral Researchers Program, RIKEN. The work of F. Nori was supported in part by the ARO, NSF grant 0726909, JSPS-RFBR Contract 12-02-92100, Grant-in-Aid for Scientific Research (S), MEXT Kakenhi on Quantum Cybernetics, and the JSPS via its FIRST program.

Y. Ota is with the Advanced Science Institute, RIKEN, Wako-shi, Saitama 351-0198, Japan (e-mail: otayuki@riken.jp).

K. Kobayashi and M. Machida are with the CCSE, Japan Atomic Energy Agency, Kashiwa, Chiba 277-8587, Japan.

T. Koyama is with the Institute for Materials Research, Tohoku University, Aoba-ku, Sendai 980-8577, Japan.

F. Nori is with the Advanced Science Institute, RIKEN, Wako-shi, Saitama 351-0198, Japan, and also with the Physics Department, University of Michigan, Ann Arbor, MI 48109-1040 USA.

Color versions of one or more of the figures in this paper are available online at http://ieeexplore.ieee.org.

Digital Object Identifier 10.1109/TASC.2013.2248871

where $\vec{A}(t,\vec{r})$ is the vector potential and $T(t,\vec{r})$ is the local temperature normalized by $T_{\rm c}$. The temporal variable is normalized by

$$t_0 = \frac{\pi\hbar}{96 k_{\rm B} T_{\rm c}} (\simeq 2.5 \times 10^{-2}\,{\rm ps}).$$

This quantity is a typical time scale of the present simulations. The dimensionless relaxation time D [21] is 1/12. The last term ζ in (1) describes fluctuations from thermal quasi-particle excitations. The complex random variable $\zeta(t,\vec{r})$ is a Gaussian white noise, with $\langle\zeta(t,\vec{r}) = 0\rangle$ and

$$\langle\zeta(t,\vec{r})\zeta^*(t',\vec{r}')\rangle = D\left(\frac{\xi_{\rm h}}{\xi}\right)^3 T(t,\vec{r})\delta(t-t')\delta^{(3)}(\vec{r}-\vec{r}')$$

$$\xi_{\rm h} = \left(\frac{4\pi k_{\rm B} T_{\rm c}}{H_{\rm c}^2}\right)^{1/3}$$

where $H_{\rm c}$ is the thermodynamic critical field at $T = 0$. The symbol $\langle\ldots\rangle$ indicates ensemble average. The prefacor $\xi_{\rm h}/\xi$ is characterized by a temperature increase per volume brought about the depairing energy density [i.e., $(H_{\rm c}^2/4\pi k_{\rm B})$].

The dimensionless Maxwell equation is

$$\kappa^2\vec{\nabla}\times\vec{B} = -\frac{\partial\vec{A}}{\partial t} + {\rm Re}\left[\Delta^*(-{\rm i}\vec{\nabla}-\vec{A})\Delta\right] + \vec{\eta}$$
$$\vec{B} = \vec{\nabla}\times\vec{A} \qquad (2)$$

where κ is the GL parameter. The magnetic field $\vec{B}$ is normalized by the upper critical field $H_{\rm c2}$ at $T = 0$. The boundary condition with respect to $\vec{B}$ is described by a function of the bias current. The term $\vec{\eta}$ is the Johnson-Nyquist noise. Each component of $\vec{\eta}$ is an independent real random field described by a Gaussian white noise, with $\langle\eta_a(t,\vec{r})\rangle = 0$ and

$$\langle\eta_a(t,\vec{r})\eta_b(t',\vec{r}')\rangle = \delta_{ab}\left(\frac{\xi_{\rm h}}{\xi}\right)^3 T(t,\vec{r})\delta(t-t')\delta^{(3)}(\vec{r}-\vec{r}').$$

In the simulations, instead of calculating $\vec{A}$ directly, we use a link variable in the lattice gauge theory [26]. This method allows stable simulations of the magnetic field.

The heat-diffusion equation is

$$C\frac{\partial T}{\partial t} - K\nabla^2 T - 2\left(\frac{\partial\vec{A}}{\partial t}\right)^2 = s + \alpha\left(\frac{T_{\rm w}}{T_{\rm c}} - T\right) f(\vec{r}) \quad (3)$$

where $s(t,\vec{r})$ is the external energy-source term. The specific heat with fixed volume, C and the thermal conductivity K are, respectively, normalized by $C_0 = k_{\rm B}/\xi_{\rm h}^3$ and $K_0 = C_0(\xi/t_0)\xi$. The last term of the right hand side describes heat absorption via a heat sink with a temperature $T_{\rm w}$ (i.e., isothermal matter with a large specific heat). The parameter α represents a coupling constant with the heat sink. We assume that $f(\vec{r}) = 1$ if $\vec{r}$ is on the surface of the system, while $f(\vec{r}) = 0$ otherwise. The derivation of (3) is shown in, e.g., [27]. We note that in (3) we drop a surface radiation term and a heat-diffusion term via a superconducting component, for simplicity.

Zotova and Vodolazov [25] simulated the two-dimensional TDGL equation with the heat-diffusion and the Maxwell equations to study dynamical responses of a SNSPD. Since their TDGL equation does not contain the Meissner current, their formulation corresponds to superfluid transport, rather than superconducting transport. Furthermore, in a superconducting nano-stripline detector, the film thickness may be an important factor for the detector characteristics [19]. Therefore, our three-dimensional TDGL approach can be important for systematically and quantitatively predicting various kinds of superconducting detectors.

TABLE I
INPUT PARAMETERES IN SIMULATIONS

Symbol	Quantity	Value
$T_{\rm c}$	superconducting transition temperature	10 K
$H_{\rm c2}$	upper critical magnetic field at 0 K	100 kG
ξ	coherent length at 0 K	5 nm
κ	Ginzburg-Landau parameter	2
$T_{\rm w}$	ambient temperature	3 K
C	dimensionless specific heat	5.0×10^{-3}
K	dimensionless thermal conductivity	3.6×10^{-3}
α	dimensionless heat-sink coupling	0.5
$t_{\rm p}$	dimensionless application time of source term	14
$r_{\rm p}$	dimensionless radius of source term	3.2

IV. PHOTON-SOURCE MODEL

In this paper, the photon-energy-source term in (3) is

$$s(t,\vec{r}) = \begin{cases} s_{\rm p}\theta(t)\theta(t_{\rm p}-t) & (\vec{r}\in\Omega) \\ 0 & ({\rm otherwise}) \end{cases} \qquad (4)$$

with a constant $s_{\rm p}$. The region Ω is a cylinder with height $d = 0.8\xi$ (i.e., film thickness) along the z-axis and radius of the top and the bottom circles on the xy-plane, $r_{\rm p}$. The skin depth of normal conductors for visible light, which is a typical wave length in single-photon detectors, is around 50 nm (i.e., visible light), which is much longer than the film thickness (4 nm). Therefore, we assume that the height of the cylinder Ω is equal to the film thickness.

The source term has a non-zero value for $t < t_{\rm p}$. We note that $r_{\rm p}$ and $t_{\rm p}$ are estimated by a typical energy scale of a single photon (~ 1 eV). The energy needed to increase the temperature in Ω up to T is $\varepsilon = CTd\pi r_{\rm p}^2$. We estimate $r_{\rm p}$ imposing that ε is equal to the photon energy and $T = T_{\rm c}$ inside Ω. Using an approximate solution of (3) [7], a time scale in which an initial spot expands to the area with the diameter $r_{\rm p}$ is evaluated. We choose this time scale as $t_{\rm p}$.

V. DYNAMICAL TRANSITION TO A RESISTIVE STATE

We show the results of our numerical simulations. The fixed input parameters in the simulations are shown in Table I. First, without the energy-source term, we obtain the I–V characteristics and find that the dimensionless critical current density is $J_{\rm c} = 0.1416$. The bias current density is normalized by the depairing current density [28], $J_{\rm d} = \sqrt{2}cH_{\rm c}/4\pi\lambda$, where λ is the penetration depth at $T = 0$ and c is the light velocity. Hereafter, we fix the bias current density as 0.135 $(= 0.95J_{\rm c})$. Under this bias current density, we numerically solve the TDGL equation coupled with the heat-diffusion and the Maxwell equations, and

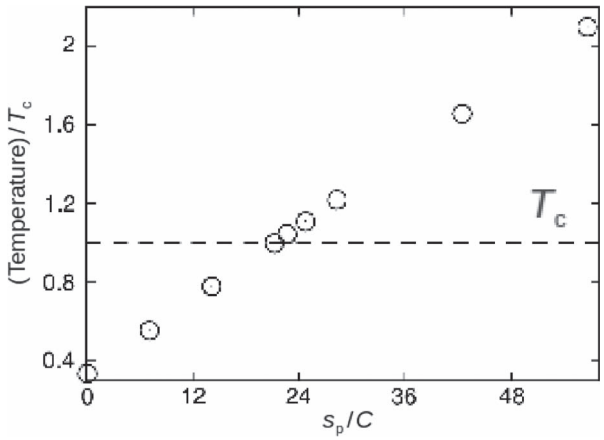

Fig. 1. Temperature increase on the top surface of an initial hotspot region. The horizontal axis corresponds to an input source magnitude $s_{\rm p}$ normalized by the dimensionless specific heat C. See (4) in the text. The horizontal dashed line indicates $T_{\rm c}$.

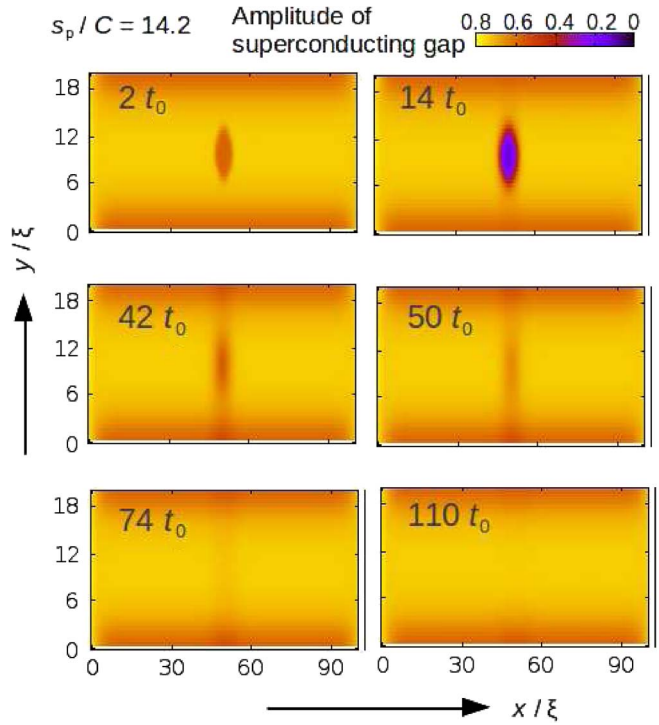

Fig. 2. Temporal behaviors of superconducting-gap amplitude for $s_{\rm p}/C = 14.2$.

obtain the stationary superconducting state after $1000t_0$. This stationary state is used as the initial state for examining the dynamical responses.

Now let us simulate the temporal behaviors of our system in the presence of the energy-source term (i.e., an incident particle) with the bias current density 0.135 ($= 0.95J_{\rm c}$). Fig. 1 shows the spatially-averaged temperature in the hotspot (with radius $r_{\rm p}$) on the top surface at the time $t_{\rm p}(= 14t_0)$. The temperature reaches $T_{\rm c}$ when $s_{\rm p}/C = 21.5$. We examine the dynamical responses of the superconducting gap amplitude, focusing on the three specific values of $s_{\rm p}/C$. First, we show the behavior when the surface temperature on the region Ω is smaller than $T_{\rm c}$, as seen in Fig. 2. We set $s_{\rm p}/C = 14.2$. A central normal-state spot appears after the source term is switched

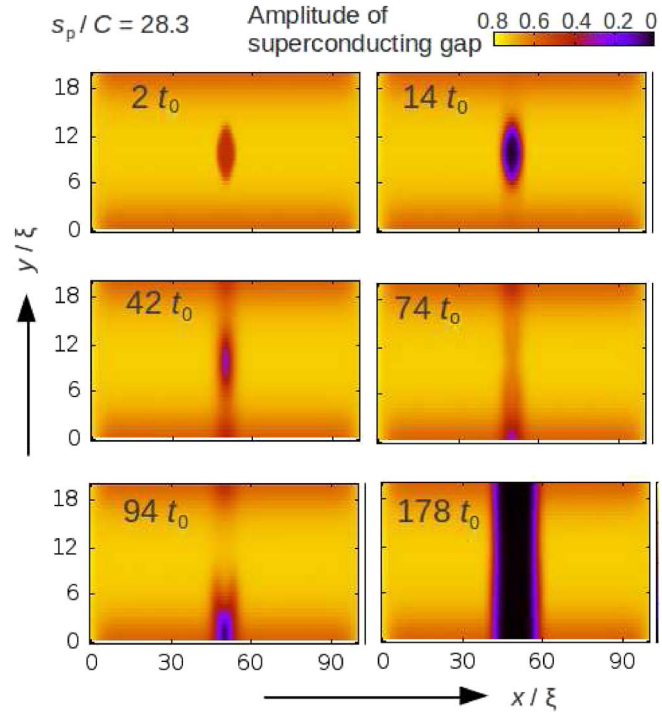

Fig. 3. Temporal behaviors of superconducting-gap amplitude for $s_{\rm p}/C = 28.3$.

off (at $14t_0$). Subsequently, a weak-superconducting strip begins expanding along y-axis. However, this strip promptly shrinks. Eventually, the system goes back to the superconducting state.

Fig. 3 shows the temporal behavior of the superconducting-gap amplitude for $s_{\rm p}/C = 28.3$. The surface temperature on Ω is close to $T_{\rm c}$, as seen in Fig. 1. The source term is added from 0 to $14t_0$. After the source term is switched off, a weak-superconducting strip begins expanding along y-axis. At $t = 42t_0$, this strip reaches both edges of the system, and a tiny normal-state region appears at the center of the system. Thus, the superconductivity in the regions sandwiched between the edge and the tiny normal-state region may easily destroy. We find that the superconducting state begins destroying at $t = 74t_0$. Eventually, a wide normal-state strip appears (at $t = 178t_0$), and the system becomes the resistive state. This normal-state strip expands to whole of the system.

We turn to the case when the surface temperature on Ω is much larger than $T_{\rm c}$ (i.e., $s_{\rm p}/C = 70.6$). Fig. 4 shows the temporal behavior of the superconducting-gap amplitude. Again, we find that a weak-superconducting strip expands along y-axis and reaches the edges of the system. In contrast to the previous case, vortex-antivortex pairs enter from both the large normal-state spot and the edges along x-axis. These pairs collides with each other, and a large normal-state stripe is produced (at $t = 110t_0$). Thus, the system is considered to be the resistive state.

Summarizing the above results, we find that the superconductor dynamically transits to its resistive state with the source magnitude higher than $T_{\rm c}$. The present method well describes a non-equilibrium transition from the superconducting state to the resistive state in superconducting detectors.

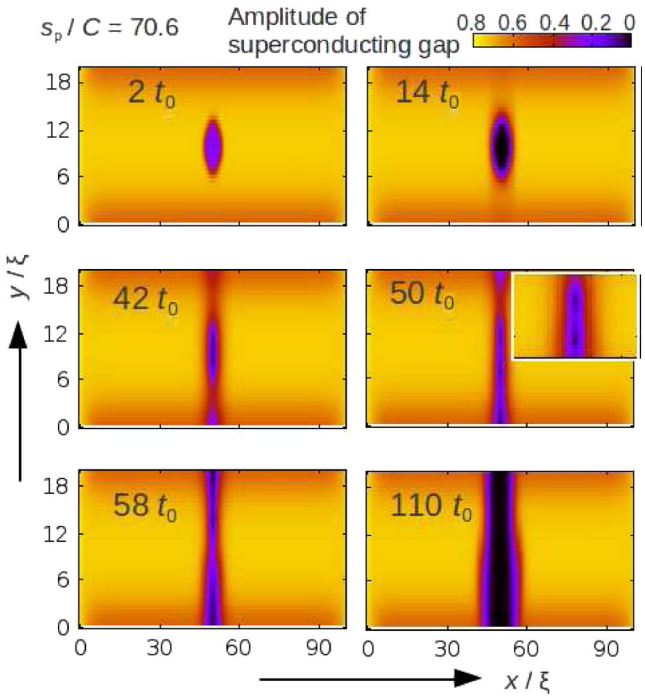

Fig. 4. Temporal behaviors of superconducting-gap amplitude for $s_{\rm p}/C = 70.6$. The inset at $t = 50t_0$ is the central region of the system. A vortex-antivortex pair appears in the central normal-state region.

VI. Effects of Heat-Sink Coupling and Noise

We discuss the applicability of the present formulation and techniques to a SNSPD from a qualitative point of view. A photon energy for the quantum key distribution is roughly estimated as 1 eV since visible light is typically used. Using the parameters in Table I, we find that $s_{\rm p}/C = 0.071$ for 1 eV. Fig. 1 indicates that the temperature on the top surface becomes higher than $T_{\rm c}$ if $s_{\rm p}/C$ is greater than 21.5. Thus, our simulation model indicates that the threshold energy is around 300 eV. We mention that this energy is the same order as the threshold energy of a superconducting nano-stripline detector for molecule/ion detections [17]–[19].

The above consideration indicates that our model has to be modified in order to reduce the discrepancy with typical single-photon's energy. To seek a clue to solve this issue, we focus on two physical parameters, the heat-sink coupling constant α and the GL parameter κ. Since it is technically difficult to use their realistic values, they are chosen so that the numerical simulations are effectively and stably performed. Hereafter, we will discuss them in further detial.

First, we focus on the heat-sink coupling. Heat transfer from a superconducting thin film to a heat sink (e.g., substrate) is associated with both electron's and phonon's contributions. In our approach, we describe this process in (3) as the linear Kapitza law with a single phenomenological constant α. This coupling constant can be roughly estimated by a typical time scale of electron-phonon interaction, as seen in, e.g., [25]. This approach may be adapted in our simulations if the quasi-particle fluctuations and the Johnson-Nyquist noise, which are necessary for reproducing a typical current-voltage characteristics near $J_{\rm c}$, are absent. Indeed, Zotova and Vodolazov [25] performed the simulations without the noise, and showed that their threshold energy was compatible with a typical energy scale of a single photon. Their electron-phonon interaction time scale $t_{\rm e-ph}$ is 17 ps, which means that $\alpha = t_0 C/t_{\rm e-ph} \simeq 0.74 \times 10^{-5}$. Our approach to determine α is that the (spatially-averaged) heat-balanced relation $-2(\partial_t \vec{A})^2 = \alpha[(T_{\rm w}/T_{\rm c}) - 1]f(\vec{r})$ fulfills without the source term. Thus, we realize stable simulations even in the presence of the noise terms. On the one hand, we can reproduce a plausible non-equilibrium superconducting state near $J_{\rm c}$. On the other hand, we require a quite large value of α. Then, this large heat-sink coupling may lead to relatively large threshold energy, compared to typical single-photon's one.

TABLE II
Threshold Energy Versus Heat-Sink Coupling

Heat-sink coupling	Noise	Threshold energy
0.5	exist	350 eV
0.38×10^{-3}	no	20 eV
0.38×10^{-5}	no	10 eV

Next, we focus on the GL parameter. In this paper, we set $\kappa = 2$ for effective numerical simulations. This value is reasonable for studying qualitative and essential features of type-II superconductor. We remark that the number of the spatial meshes for a three-dimensional GL simulation is roughly described by a function of $(a^2)^3 = a^6$ when κ becomes $a\kappa$. The penetration depth of a thin film of NbN is around 300 nm, which means that $\kappa \simeq 60$. Since we fix $H_{\rm c2}$ as an experimental value, $H_{\rm c}$ in the simulations is much larger than in the realistic materials. Thus, the temperature increase per volume $(\xi_{\rm h}/\xi)^3$ is underestimated in the simulations, since $(\xi_{\rm h}/\xi)^3 \propto H_{\rm c}^{-2}$.

Let us perform the simulation simply dropping the noise terms in order to examine the effect of the heat-sink coupling in our approach. A simulation without the noise may correspond to clean-limit superconducting transport. We reduce the heat-sink coupling to a similar value to [25]. We summarize the results for the threshold energy (i.e., minimum energy for the occurrence of a large normal-state stripe) varying the heat-sink coupling in Table II. We find that the threshold energy becomes a much smaller value, compared to the previous simulation. The development of a simulation method with noise and weak heat-sink coupling is a future issue.

Another important issue is to develop a simulation method for a realistic GL parameter. Although it is difficult for the current computational resources to do simulations for $\kappa > 10$, we can effectively treat large-κ cases by varying the magnitude of the quasi-particle fluctuations. The diffusion constant of the Gaussian white noise ζ is characterized by the factor $\xi_{\rm h}/\xi$. This factor depends on κ, since the thermodynamic critical magnetic field $H_{\rm c}$ is determined by $H_{\rm c2}$ and κ. Thus, the change of the diffusion constant of ζ effectively corresponds to the change of κ. As a result, we expect that the temperature increase is more drastic than in the previous simulation. Furthermore, as shown above, weak heat-sink coupling has a positive effect for reducing the threshold energy. We vary the heat-sink coupling on the top surface. This setting may correspond to the case when the bottom surface of a superconducting thin film touches

TABLE III
THRESHOLD ENERGY FOR STRONG QUASI-PARTICLE FLUCTUATION

Effective Ginzburg-Landau parameter	Heat-sink coupling on top surface	Threshold energy
2	0.05	60 eV
60	0.05	50 eV
60	0.48	40 eV

on a substrate, while the top surface not. We summarize the results in Table III. We find again that the threshold energy decreases. Hence, we expect that via optimization about the fluctuation strength and the heat-sink coupling our approach works in a SNSPD.

VII. CONCLUSION

We numerically simulated the superconducting detector made by a superconducting thin film using the TDGL equation coupled with the heat-diffusion and the Maxwell equations. When the incident particle brings a large temperature increase, a superconductor dynamically transits to its resistive state. Depending on the source energy, we found two distinct types of the superconducting-breaking behaviors. Finally, we discussed the applicability of the present method to SNSPDs. Tuning either the heat-sink coupling and the quasi-particle fluctuation can lead to a realistic threshold energy for SNSPDs.

ACKNOWLEDGMENT

The authors thank A. L. Rakhmanov, A. O. Sboychakov, T. Yamashita, S. Miki, H. Terai, Z. Wang, M. Fujiwara, and M. Sasaki for their very useful comments. The calculations were performed by using the RIKEN Integrated Cluster of Clusters facility.

REFERENCES

[1] K. D. Irwin and G. C. Hilton, "Transition-edge sensors," in *Cryogenic Particle Detection*, C. Enss, Ed. Berlin, Germany: Springer-Verlag, 2005, pp. 63–149.

[2] L. Ozyuzer, A. E. Koshelev, C. Kurter, N. Gopalsami, Q. Li, M. Tachiki, K. Kadowaki, T. Yamamoto, H. Minami, H. Yamaguchi, T. Tachiki, K. E. Gray, W. K. Kwok, and U. Welp, "Emission of coherent THz radiation from superconductors," *Science*, vol. 318, no. 5854, pp. 1291–1293, Nov. 2007.

[3] S. Savel'ev, V. A. Yampol'skii, A. L. Rakhmanov, and F. Nori, "Terahertz Josephson plasma waves in layered superconductors: Spectrum, generation, nonlinear, and quantum phenomena," *Rep. Prog. Phys.*, vol. 73, no. 2, pp. 026501-1–026501-49, Feb. 2010.

[4] M. N. Wilson, *Superconducting Magnets*. New York, NY, USA: Oxford Univ. Press, 1983.

[5] J. Q. You and F. Nori, "Superconducting circuits and quantum information," *Phys. Today*, vol. 58, no. 11, pp. 42–47, Nov. 2005.

[6] J. Q. You and F. Nori, "Atomic physics and quantum optics using superconducting circuits," *Nature*, vol. 474, no. 7353, pp. 589–597, Jun. 2011.

[7] A. M. Kadin and M. W. Johnson, "Nonequilibrium photon-induced hotspot: A new mechanism for photodetection in ultrathin metallic films," *Appl. Phys. Lett.*, vol. 69, no. 25, pp. 3938–3940, Dec. 1996.

[8] A. D. Semenov, G. N. Gol'tsman, and A. A. Korneev, "Quantum detection by current carrying superconducting film," *Phys. C, Supercond.*, vol. 351, no. 4, pp. 349–356, Apr. 2001.

[9] G. N. Gol'tsman, O. Okunev, G. Chulkova, A. Lipatov, A. Semenov, K. Smirnov, B. Voronov, A. Dzardanov, C. Williams, and R. Sobolewski, "Picosecond superconducting single-photon optical detector," *Appl. Phys. Lett.*, vol. 79, no. 6, pp. 705–707, Aug. 2001.

[10] J. K. W. Yang, A. J. Kerman, E. A. Dauler, V. Anant, K. M. Rosfjord, and K. K. Berggren, "Modeling the electrical and thermal response of superconducting nanowire single-photon detectors," *IEEE Trans. Appl. Supercond.*, vol. 17, no. 2, pp. 581–585, Jun. 2007.

[11] S. Miki, M. Takeda, M. Fujiwara, M. Sasaki, and Z. Wang, "Compactly packaged superconducting nanowire single-photon detector with an optical cavity for multichannel system," *Opt. Exp.*, vol. 17, no. 26, pp. 23557–23564, Dec. 2009.

[12] M. Ejrnaes, A. Casaburi, O. Quaranta, S. Marchetti, A. Gaggero, F. Mattioli, R. Leoni, S. Pagano, and R. Cristiano, "Characterization of parallel superconducting nanowire single photon detectors," *Supercond. Sci. Technol.*, vol. 22, no. 5, pp. 055006-1–055006-7, May 2009.

[13] T. Yamashita, S. Miki, W. Qiu, M. Fujiwara, M. Sasaki, and Z. Wang, "Temperature dependence performances of superconducting nanowire single-photon detectors in an ultralow-temperature region," *Appl. Phys. Exp.*, vol. 3, no. 10, pp. 102502-1–102502-3, Sep. 2010.

[14] M. Machida, T. Koyama, M. Kato, and T. Ishida, "Direct numerical experiments for neutron detection using superconductor MgB_2," *Nucl. Instrum. Methods Phys. Res. A, Accel. Spectrom. Detect. Assoc. Equip.*, vol. 529, no. 1–3, pp. 409–412, Aug. 2004.

[15] M. Machida, T. Koyama, M. Kato, and T. Ishida, "Direct numerical simulation on non-equilibrium superconducting dynamics after neutron capture in MgB_2 superconductor," *Nucl. Instrum. Methods Phys. Res. A, Accel. Spectrom. Detect. Assoc. Equip.*, vol. 559, no. 2, pp. 594–596, Apr. 2006.

[16] M. Machida, T. Kano, T. Koyama, M. Kato, and T. Ishida, "Direct numerical simulations for non-equilibrium superconducting dynamics at the transition edge: Simulation for MgB_2 neutron detectors," *J. Low Temp. Phys.*, vol. 151, no. 1/2, pp. 58–63, Apr. 2008.

[17] M. Ohkubo, "Superconducting detectors for particles from atoms to proteins," *Phys. C, Supercond.*, vol. 468, no. 15–20, pp. 1987–1991, Sep. 2008.

[18] K. Suzuki, S. Miki, Z. Wang, and M. Ohkubo, "Time resolution improvement of superconducting NbN stripline detectors for time-of-flight mass spectrometry," *Appl. Phys. Exp.*, vol. 1, no. 3, pp. 031702-1–031702-3, Mar. 2008.

[19] K. Suzuki, S. Shiki, M. Ukibe, M. Koike, S. Miki, Z. Wang, and M. Ohkubo, "Hot-spot detection model in superconducting nano-stripline detector for keV ions," *Appl. Phys. Exp.*, vol. 4, no. 8, pp. 083101-1–083101-3, Aug. 2011.

[20] R. Kato, Y. Enomoto, and S. Maekawa, "Effects of the surface boundary on the magnetization process in type-II superconductors," *Phys. Rev. B, Condens. Matter*, vol. 47, no. 13, pp. 8016–8024, Apr. 1993.

[21] M. Machida and H. Kaburaki, "Direct simulation of the time-dependent Ginzburg-Landau equation for type-II superconducting thin film: Vorex dynamics and V-I characteristics," *Phys. Rev. Lett.*, vol. 71, no. 19, pp. 3206–3209, Nov. 1993.

[22] I. Shapiro, E. Pechenik, and B. Ya. Shapiro, "Recovery of superconductivity in a quenched mesoscopic domain," *Phys. Rev. B, Condens. Matter*, vol. 63, no. 18, pp. 184520-1–184520-10, May 2001.

[23] N. Nakai, N. Hayashi, and M. Machida, "Direct numerical confirmation of pinning-induced sign change in the superconducting Hall effect in type-II superconductors," *Phys. Rev. B, Condens. Matter*, vol. 83, no. 2, pp. 024507-1–024507-5, Jan. 2011.

[24] J. R. Clem, Y. Mawatari, G. R. Berdiyorov, and F. M. Peeters, "Predicted field-dependent increase of critical currents in asymmetric superconducting nanocircuits," *Phys. Rev. B, Condens. Matter*, vol. 85, no. 14, pp. 144511-1–144511-16, Apr. 2012.

[25] A. N. Zotova and D. Y. Vodolazov, "Photon detection by current-carrying superconducting film: A time-dependent Ginzburg-Landau approach," *Phys. Rev. B, Condens. Matter*, vol. 85, no. 2, pp. 024509-1–024509-9, Jan. 2012.

[26] K. G. Wilson, "Confinement of quarks," *Phys. Rev. D, Part. Fields*, vol. 10, no. 8, pp. 2445–2459, Oct. 1974.

[27] K. Kobayashi, Y. Ota, and M. Machida, "Numerical experiments of Joule heat damage in superconducting transport," *Phys. Proc.*, vol. 27, pp. 120–123, 2012.

[28] M. Thinkham, *Introduction to Superconductivity*, 2nd ed. New York, NY, USA: Dover, 2004, ch. 4.